PNAS RESEARCH ARTICLE | BIOCHEMISTRY

C-terminal glutamine acts as a C-degron targeted by E3 ubiquitin ligase TRIM7

Yawei Ru[a,b,1], Xiaojie Yan[a,c,1], Bing Zhang[c,1], Lili Song[d,1], Qiqi Feng[c], Chen Ye[d], Zhili Zhou[d], Zhenzhen Yang[c], Yao Li[c], Zhenjian Zhang[d], Qianqian Li[d], Wenyi Mi[d,2], and Cheng Dong[a,c,2]

Edited by Christopher Lima, Memorial Sloan Kettering Cancer Center, New York, NY; received March 15, 2022; accepted June 6, 2022

The exposed N-terminal or C-terminal residues of proteins can act, in cognate sequence contexts, as degradation signals (degrons) that are targeted by specific E3 ubiquitin ligases for proteasome-dependent degradation by *N*-degron or C-degron pathways. Here, we discovered a distinct C-degron pathway, termed the Gln/C-degron pathway, in which the B30.2 domain of E3 ubiquitin ligase TRIM7 ($TRIM7^{B30.2}$) mediates the recognition of proteins bearing a C-terminal glutamine. By determining crystal structures of $TRIM7^{B30.2}$ in complexes with various peptides, we show that $TRIM7^{B30.2}$ forms a positively charged binding pocket to engage the "U"-shaped Gln/C-degron. The four C-terminal residues of a substrate play an important role in C-degron recognition, with C-terminal glutamine as the principal determinant. In vitro biochemical and cellular experiments were used to further analyze the substrate specificity and selective degradation of the Gln/C-degron by TRIM7.

degron | protein degradation | E3 ubiquitin ligase | TRIM7 | crystal structure

Significance

Targeted protein degradation protects cells from disturbance of abnormal or heterologous proteins. E3 ubiquitin ligase TRIM7 is identified as an antiviral effector that restricts enterovirus replication through targeting of the viral 2BC protein for proteasome-dependent degradation. Here, we found that TRIM7 specifically recognizes a general C-terminal glutamine residue by its B30.2 domain and targets 2BC protein bearing a Gln/C-degron for degradation through the Gln/C–degron pathway. We present crystal structures of $TRIM7^{B30.2}$ bound to various peptides ending with C-terminal glutamine. By combining mutagenesis and biochemical analyses, we delineated the recognition mechanism of Gln/C-degron by $TRIM7^{B30.2}$.

Protein degradation is an evolutionarily conserved process for protein quality control and cellular homeostasis (1–4). Endogenous cellular proteins, as well as proteins that are encoded during infections by bacterial or viral chromosomes, can also be substrates for selective degradation (2, 5). Perturbations of protein degradation can lead to metabolic imbalances and disturbance of cell proliferation and differentiation and are prominent as causes of many human diseases (6–8).

The ubiquitin (Ub)-proteasome system (UPS) is a major system for selective degradation of intracellular proteins. UPS initially targets a protein substrate through an E1-E2-E3 enzymatic cascade that leads to polyubiquitination of the protein, followed by its recognition (in part through a poly-Ub chain) and processive degradation by the 26S proteasome (9, 10). In the mammalian UPS, one or more of about 800 E3 Ub ligases initially targets a protein substrate by recognizing its specific degradation signal (degrons). The latter is usually composed of short linear sequence motifs (11–13). The first degrons, discovered in 1986 and termed *N*-degrons, comprised specific N-terminal (Nt) residues of substrate proteins (14). These *N*-degrons were recognized by a specific proteolytic system initially termed the *N*-end rule pathway and later renamed the *N*-degron pathway (15). Analogous C-terminal (Ct) degrons are recognized by specific C-degron pathways (16, 17). Specific sets of *N*-degron and C-degron pathways have emerged as a major part of the UPS (15). Specific E3 Ub ligases that recognize *N*-degrons and C-degrons are called *N*-recognins and C-recognins, respectively (15).

The currently known eukaryotic *N*-degron pathways are the Arg/*N*-degron pathway, the Ac/*N*-degron pathway, the Pro/*N*-degron pathway, the Gly/*N*-degron pathway, and the fMet/*N*-degron pathways (18–20). The corresponding E3 *N*-recognins, including UBR1 and UBR2 in the UBR family of E3s (21, 22), GID4 and GID10 in the GID family of E3s (23–26), and ZYG11B and ZER1 in the Cullin-RING family (27), have been explored by structural biology. *N*-degron pathways participate in numerous biological processes, including regulation of anti-apoptosis, mitochondrial quality control, cardiovascular development, neurogenesis, spermatogenesis, and various functions of the immune system (6, 28–30). For example, by "decorating" infecting cytosolic bacteria with Ub moieties, specific E3 Ub ligases can play a role in the clearance of bacterial pathogens (5, 31). In addition, in the Gly/*N*-degron pathway, CRL2ZER1/ZYG11B has been demonstrated to be accountable for 3C protease-mediated activation of the NLRP1-dependent inflammasome during human rhinovirus infection (32).

Analogous C-degron pathways were discovered more recently (15, 33). In particular, specific Cullin-RING E3 Ub ligases (CRLs) have been identified as C-recognins that recognize distinct C-degrons and target proteins bearing these degrons for degradation (17, 18, 34). Tripartite motif (TRIM) proteins, a branch of the RING protein family, comprise a large set of E3 Ub ligases (35, 36). TRIM7 was recently reported to inhibit

Author contributions: W.M. and C.D. designed research; Y.R., X.Y., B.Z., L.S., Q.F., C.Y., Z.Zhou, Z.Y., Y.L., Z.Zhang, and Q.L. performed research; X.Y., B.Z., W.M., and C.D. analyzed data; and X.Y., B.Z., W.M., and C.D. wrote the paper.

The authors declare no competing interest.

This article is a PNAS Direct Submission.

[1]Y.R., X.Y., B.Z., and L.S. contributed equally to this work.

[2]To whom correspondence may be addressed. Email: wenyi.mi@tmu.edu.cn or dongcheng@tmu.edu.cn.

This article contains supporting information online at http://www.pnas.org/lookup/suppl/doi:10.1073/pnas.2203218119/-/DCSupplemental.

Published July 22, 2022.

enterovirus replication by targeting the 2BC protein (proteolytic precursor of 2C, an adenosinetriphosphatase (ATPase)/helicase that is critical for viral RNA replication in coxsackievirus B3 [CVB3]) for proteasome-mediated degradation (37). Here, we discovered that TRIM7 targets 2BC for degradation by recognizing its Ct-glutamine residue (a Gln/C-degron). We further uncovered the molecular mechanism underlying TRIM7-mediated recognition of Gln/C-degron via biochemistry and structural biology. This study expands our understanding of C-degron pathways and illustrates future strategies for the structure-based design of chemical probes for modulating protein degradation.

Results

The PRY-SPRY Domain of TRIM7 Recognizes the Gln/C-Degron. Nearly all TRIM family proteins have conserved Nt-domains composed of RING, B-box, and Coiled-coil domain (named TRIM/RBCC motif), while the Ct-domains are extremely variable and endow TRIM family proteins with functional specificity (36, 38). Among these proteins, TRIM7 is a typical E3 ligase containing an Nt-TRIM motif followed by a Ct–PRY-SPRY domain (also termed B30.2 domain) (Fig. 1*A*). Recently, TRIM7 was shown to target human enterovirus CVB3 2BC protein for ubiquitination and proteasomal degradation, and the Ct-polypeptide of viral 2C protein is important for its binding to the TRIM7 B30.2 domain (hereafter referred to as $TRIM7^{B30.2}$) (37).

To further explore the interaction between TRIM7 and 2C, we purified $TRIM7^{B30.2}$ and 2C protein as well as synthesized a nonapeptide corresponding to the Ct-sequence of 2C (GATLEALFQ), then performed an isothermal titration calorimetry (ITC) assay to examine their binding affinities. Notably, the results showed that 2C peptide is sufficient to mediate the interaction with $TRIM7^{B30.2}$ with a K_D value of 1.9 μM, which is comparable to that of 2C protein (K_D = 4.8 μM) (Fig. 1*B* and *C*). Thus, we speculated that 2C protein might utilize a limited Ct-motif for its recognition by $TRIM7^{B30.2}$. To test this hypothesis, we set out to map the minimal length of the 2C peptide required for recognition of $TRIM7^{B30.2}$. We synthesized a series of peptides based on a 2C peptide ranging from two to nine residues in length. ITC experiments suggest that a four-residue peptide retained relatively strong binding ability, albeit five-residue or longer peptides exhibited slightly increased binding affinity (Fig. 1*D*). In contrast, the three-residue peptide displayed eightfold decreased binding affinity and the two-residue peptide resulted in weak binding (Fig. 1*D*), indicating that the four Ct-residues of this 2C peptide are mainly responsible for its interaction with $TRIM7^{B30.2}$.

To ascertain the key elements of 2C required for $TRIM7^{B30.2}$ binding, we synthesized alanine (Ala) substitutions of 2C peptide and examined their binding affinities with $TRIM7^{B30.2}$. Remarkably, substitution of the Q−1 (Q−1 refers to the Gln at −1 position) with Ala caused a complete loss of binding (Fig. 1*E*), suggesting the key role of Ct-Gln in $TRIM7^{B30.2}$ binding. The other position substitutions exhibited a modest effect on $TRIM7^{B30.2}$ binding, although F−2 substitution reduced the binding affinity by eightfold (Fig. 1*E*), indicating an accessory role of the residues upstream of Q−1. This result suggests that the Ct-Gln of 2C protein may act as a C-degron (Gln/C-degron) targeted by TRIM7 for selective degradation.

TRIM7 has also been shown to interact with GN1 (glycogenin-1) (39) and mediate the ubiquitination of RACO-1 (RING domain AP-1 coactivator 1) (40). Interestingly, sequence alignments indicated that 2C, GN1, and RACO-1 possess a conserved Ct-Gln (*SI Appendix*, Fig. S1*A*), raising the possibility that there may be a general Ct-Gln–containing sequence context for $TRIM7^{B30.2}$ recognition. To this end, we synthesized the other two nonapeptides corresponding to the Ct-sequences of GN1 (KRKLDTYLQ) and RACO-1 (NLGLSMLLQ) and then performed ITC assays to examine their binding affinities. The results showed that $TRIM7^{B30.2}$ could readily bind to these two peptides, with K_D values of 2.7 μM and 3.1 μM, respectively (*SI Appendix*, Fig. S1*B* and *C*). Furthermore, we generated Ala replacements of the Ct-Gln upon GN1 and RACO-1 and examined their interactions with $TRIM7^{B30.2}$ by ITC. Correspondingly, the Q−1A mutant peptides completely lost their $TRIM7^{B30.2}$-binding activities (*SI Appendix*, Fig. S1*D* and *E*). These results suggest that the TRIM7-mediated interactions of GN1 and RACO-1 are also dependent on the recognition of their Ct-Gln.

To further verify this notion, we expressed that glutathione S-transferase (GST)–fused nonapeptide corresponding to the Ct-sequences of 2C, GN1, and RACO-1 and then performed GST pull-down assays with purified $TRIM7^{B30.2}$. The results showed that these three GST-fused peptides were able to pull down $TRIM7^{B30.2}$, whereas Ala mutation of Q−1 entirely abrogated their binding (*SI Appendix*, Fig. S1*F*). This result reemphasized the essential role of Ct-Gln in recognition by $TRIM7^{B30.2}$, which was in agreement with our ITC analysis (Fig. 1*C* and *E* and *SI Appendix*, Fig. S1*B–E*). Together, our results suggest that $TRIM7^{B30.2}$ recognizes a Gln/C-degron and that a four-residue C-degron primarily mediates its high-affinity binding.

Structure of $TRIM7^{B30.2}$ Bound to Gln/C-Degron. To gain molecular insights into TRIM7-substrate recognition, we determined the crystal structures of $TRIM7^{B30.2}$ in complex with 2C, GN1, or RACO-1 peptide at high resolution (*SI Appendix*, Fig. S2*A–C*). The electron density maps of these three peptides were well defined in our complex structures (*SI Appendix*, Fig. S2*D–F*). Crystallographic data and refinement statistics are summarized in Table 1. As expected, TRIM7 adopted a typical PRY-SPRY domain and formed a globular β-sandwich. This β-sandwich structure was composed of two antiparallel β-sheets (sheet A and sheet B) and several various-length loops. Therein, sheet B formed a slightly convex surface with seven strands (β1, β2, β4, β9, β10, β11, and β13) and sheet A formed a relatively concave surface with six strands (β3, β5, β6, β7, β8, and β12) on the opposite side (Fig. 2*A* and *B*). With peripheral covering of three hairpin loops linking β2-β3, β5-β6, and β7-β8, the concave surface strands of β3, β12, β5, and β6 formed a deep groove (Fig. 2*A* and *B*). Structural analysis suggests that this groove pocket took main responsibility for the recognition of the Gln/C-degron, in which the Ct-Gln lies flatwise at the bottom of the binding pocket (Fig. 2*A*), spanning across PRY (β3) and SPRY (β12, β5, and β6) (Fig. 2*B*). Although approximately half of the TRIM family proteins carry PRY-SPRY domain for recognition of specific substrates (35, 38), evolutionary sequence conservation analysis of different PRY-SPRY domains revealed that the substrate recognition pockets were not conserved (*SI Appendix*, Fig. S3), implying a specific recognition mode of Gln/C-degron by TRIM7 in TRIM family proteins.

Superposition of the structures of $TRIM7^{B30.2}$ bound to different peptides revealed that the overall structures of $TRIM7^{B30.2}$ adopted a rigid conformation (Fig. 2*C*). Interestingly, all three peptides folded into a flat "U"-shaped structure consisting of the four Ct-residues (Fig. 2*C* and *D*). It is worth noting that Q−1 displays an absolutely identical orientation nestling in the binding pocket (Fig. 2*D*), implicating a conservative conformation of Ct-Gln recognized by $TRIM7^{B30.2}$. Based on the complex structure, the free Ct-Gln was buried at the bottom of a positively

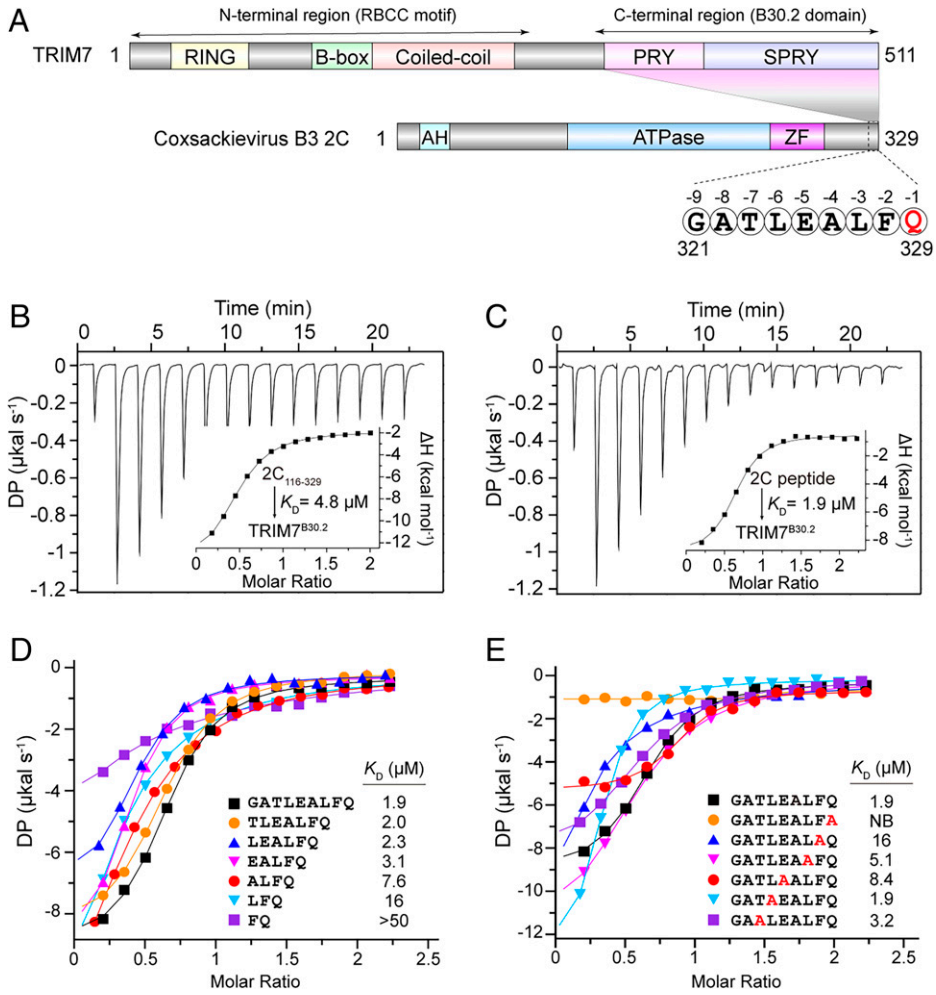

Fig. 1. The PRY-SPRY (B30.2) domain of TRIM7 mediates recognition of the Gln/C-degron. (*A*) Domain architecture of human TRIM7 and coxsackievirus 2C. AH, arfaptin homology; RING, really interesting new gene; ZF, zinc finger. (*B*) ITC titration and fitting curve of TRIM7$^{B30.2}$ with 2C protein (residues 116 to 329). (*C*) ITC titration and fitting curve of TRIM7$^{B30.2}$ with 2C peptide (residues 321 to 329, sequence: GATLEALFQ). (*D*) ITC fitting curves of TRIM7$^{B30.2}$ with variable lengths of the 2C peptide. The corresponding peptide lengths, sequences, and binding affinities are indicated. (*E*) ITC fitting curves of TRIM7$^{B30.2}$ titrated by a series of peptides with position substitutions. The corresponding peptide sequences and binding affinities are indicated. DP, differential power; NB, no binding.

charged binding pocket of TRIM7$^{B30.2}$ (P-1 pocket) (Fig. 2*E*). Meanwhile, the −2 to −4 residues were arranged at the periphery of the groove by a network of molecular interactions (Fig. 2*E*). Instead, the upstream residues of −4 position were more exposed to solvent (Fig. 2*E*) and thus were less important for the TRIM7$^{B30.2}$ binding, which was in line with our ITC observations (Fig. 1*D* and *E*). Overall, our structures demonstrate that TRIM7 utilized the PRY and SPRY domain, forming a positively charged pocket to engage the four Ct-residues.

Key Determinants of Ct-Gln. Since all three of these peptides bound to TRIM7$^{B30.2}$ shared conserved features (*SI Appendix*, Fig. S4*A*–*C*), hereafter we selected TRIM7$^{B30.2}$-2C to illustrate the molecular details in Gln/C-degron recognition. In light of the complex structure, Ct-Gln made intricate interactions with the surrounding TRIM7$^{B30.2}$ residues (Fig. 3*A* and *SI Appendix*, Fig. S4*A*). First, the carbonyl oxygen atom of Q−1 was coordinated by three hydrogen bonds, two from side-chain amino groups of Arg385 and Asn383 and one mediated by one water molecule (Fig. 3*A* and *B*). Simultaneously, the hydroxyl oxygen atom of Q−1 was further stabilized by hydrogen bonds with the imino group of Arg385 and the hydroxyl group of Ser499 (Fig. 3*A* and *B*). Our ITC assay results showed that a Ct-amidation of the carboxyl group completely abolished Gln/C-degron binding (Fig. 3*H*), highlighting the crucial role of the free Ct-Gln in TRIM7$^{B30.2}$ recognition.

Moreover, the side-chain carboxamide of Q−1 not only formed three hydrogen bonds with the hydroxyl group of Ser499, carbonyl oxygen atom of Gly408, and side-chain carboxamide of Gln436, but it also made indirect contacts with Gly408, Trp409, and Leu437, bridged by a water molecule (Fig. 3*A* and *B*). As a result, Q−1 fit tightly into the positively charged binding groove of TRIM7$^{B30.2}$ (Fig. 2*E*). Not surprisingly, neither removal of Q−1 nor mutation of Q−1 to glutamic acid (E−1) or Ala (A−1), even analogous Asn (N−1), was capable of binding to TRIM7$^{B30.2}$ by our ITC analysis (Fig. 3*H*). Aside from hydrogen bonding interactions, the backbone of Q−1 is closely buttressed by the benzyl group of neighboring Phe426 through formation of C-H···π interaction. Therefore, adding an additional valine—even the smallest glycine residue—following Q−1 could not be tolerated in this limited binding pocket (Fig. 3*H*). Thus, this unique binding mode indicates that a free Ct-Gln is indispensable for the recognition of the Gln/C-degron by TRIM7$^{B30.2}$.

Preference of Other Positions in the Gln/C-Degron. The main chain of F−2 was shown to be oriented by three hydrogen bonds with Thr384 and a water molecule (Fig. 3*C*). Specifically,

Table 1. Data collection and refinement statistics of TRIM7$^{B30.2}$

	TRIM7$^{B30.2}$-2C	TRIM7$^{B30.2}$-GN1	TRIM7$^{B30.2}$–RACO-1
PDB accession number	7Y3A	7Y3B	7Y3C
Data collection			
Space group	P 2_1	P 6_5	P 6_5
Cell dimensions			
a, *b*, *c* (Å)	79.228, 53.644, 80.999	79.768, 79.768, 52.229	79.898, 79.898, 53.108
α, β, γ (°)	90.00, 119.21, 90.00	90.00, 90.00, 120.00	90.00, 90.00, 120.00
Resolution (Å)	70.70 to 1.70 (1.80 to 1.70)*	41.66 to 1.76 (1.82 to 1.76)	69.19 to 1.71 (1.80 to 1.71)
R_{sym} or R_{merge}	0.046 (0.140)	0.132 (1.229)	0.166 (2.304)
$I/\sigma I$	23.73 (8.55)	20.08 (1.60)	12.90 (2.20)
Completeness (%)	99.4 (99.2)	99.87 (99.1)	92.9 (85.3)
Redundancy	12.1 (3.0)	18.1 (9.5)	11.2 (1.50)
Refinement			
Resolution (Å)	26.65 to 1.41 (1.76 to 1.70)	39.88 to 1.76 (1.82 to 1.76)	39.95 to 1.71 (1.77 to 1.71)
No. reflections	65,561 (6,527)	18,829 (1,870)	19,612 (1,781)
R_{work}/R_{free}	0.1319/0.1556	0.1602/0.1832	0.1627/0.1972
No. atoms			
Protein	4,391	1,420	1,466
Water	781	180	151
B-factors			
Protein	12.2	21.3	24.7
Water	26.5	32.7	34.9
rmsd			
Bond lengths (Å)	0.008	0.008	0.007
Bond angles (°)	1.03	0.98	0.98

*Values in parentheses are for highest-resolution shell.

F−2 was lined with a mixed positively charged and hydrophobic surface in which the benzyl group of F−2 was sandwiched by Arg354 and Leu423 of TRIM7$^{B30.2}$ via the cation–π interaction and hydrophobic interaction, respectively. On the other side, the side-chain methyl group of Thr382 donated additional hydrophobic interaction (Fig. 3*C*). Consequently, this specific contact surface was more suitable for docking a bulky hydrophobic residue. Indeed, substitution of F−2 with an acidic residue (D−2) or an Ala residue (A−2) decreased the binding affinity by 8 to 15 folds (Fig. 3*I*). However, replacement of F−2 with a positively charged residue (R−2) or polar serine (S−2), which repelled the electrical potential surface, greatly diminished the binding affinity by more than 50-fold (Fig. 3*I*), indicating that the −2 position prefers bulky hydrophobic residues in the Gln/C-degron context.

The side chain of L−3 formed a strong hydrophobic interaction with Leu423 of TRIM7$^{B30.2}$ (Fig. 3*D*). Additionally, the main chain of L−3 was anchored by three water-mediated hydrogen bonds. ITC results revealed that TRIM7$^{B30.2}$ could tolerate most kinds of amino acids at the −3 position, with strong binding of a hydrophobic residue (Fig. 3*J*). Likewise, the −4 and −5 positions were mainly accommodated by water-mediated hydrogen bonds (Fig. 3*E* and *F*). Therefore, variable residues could be allowed at these positions of the Gln/C-degron (Fig. 3*K*).

Interestingly, other than intermolecular interactions, intramolecular hydrogen bonds also played an important role in conformational stability of the U shape of the Gln/C-degron by formation of a hydrogen bond network among the main chain of the four Ct-residues (Fig. 3*G*). Since the intramolecular interactions were mainly maintained by the backbone groups of the Gln/C-degron (Fig. 3*G*), it is not surprising that these residues forming the U shape were not strictly conserved except for the Ct-Gln in the Gln/C-degron.

In sum, the four Ct-residues of the Gln/C-degron predominantly determine the interactions with TRIM7$^{B30.2}$ by hydrogen bonding and hydrophobic interactions. Although the Ct-Gln acts as the key determinant residue of C-degron binding, the −2 and −3 positions, which prefer hydrophobic residues, also exhibited important roles for Gln/C-degron recognition. In addition, the intramolecular interactions of the main chain are also required for maintenance of the U-shaped conformation of the Gln/C-degron recognized by TRIM7$^{B30.2}$.

Confirmation of Recognition of the Gln/C-Degron by TRIM7 in Cells. To further confirm recognition of the Gln/C-degron by TRIM7 in cells, we individually expressed GFP-fused 2C, GN1, or RACO-1 peptide together with HA-tagged TRIM7 in HEK293T cell lines. Cells were treated with MG132 (10 μM) for 6 h at 24 h after transfection, and coimmunoprecipitation (Co-IP) experiments were performed to examine their interactions with full-length HA-tagged TRIM7. As expected, we were able to detect appreciable binding of TRIM7 with these three peptides, but not the Ala mutants of Q−1 (Fig. 4*A*–*C*). These observations were consistent with our previous ITC and GST–pull-down analyses (Fig. 1*E* and *SI Appendix*, Fig. S1*D*–*F*). Hence, we concluded that TRIM7 is a C-recognin that specifically targets the Gln/C-degron.

To determine the importance of key residues of TRIM7$^{B30.2}$ in mediating Gln/C-degron recognition, we generated a series of TRIM7$^{B30.2}$ Ala mutants and performed ITC experiments to examine their binding affinities toward the 2C peptide. Unsurprisingly, the binding capabilities of these TRIM7 mutants were substantially compromised (Fig. 4*D*). In particular, L423A mutation of TRIM7$^{B30.2}$ displayed 15-fold decreased binding affinity for 2C, while this binding was completely abolished by L423D mutation, indicating that hydrophobic contact is important for the binding of −2 and −3 position residues of the 2C peptide.

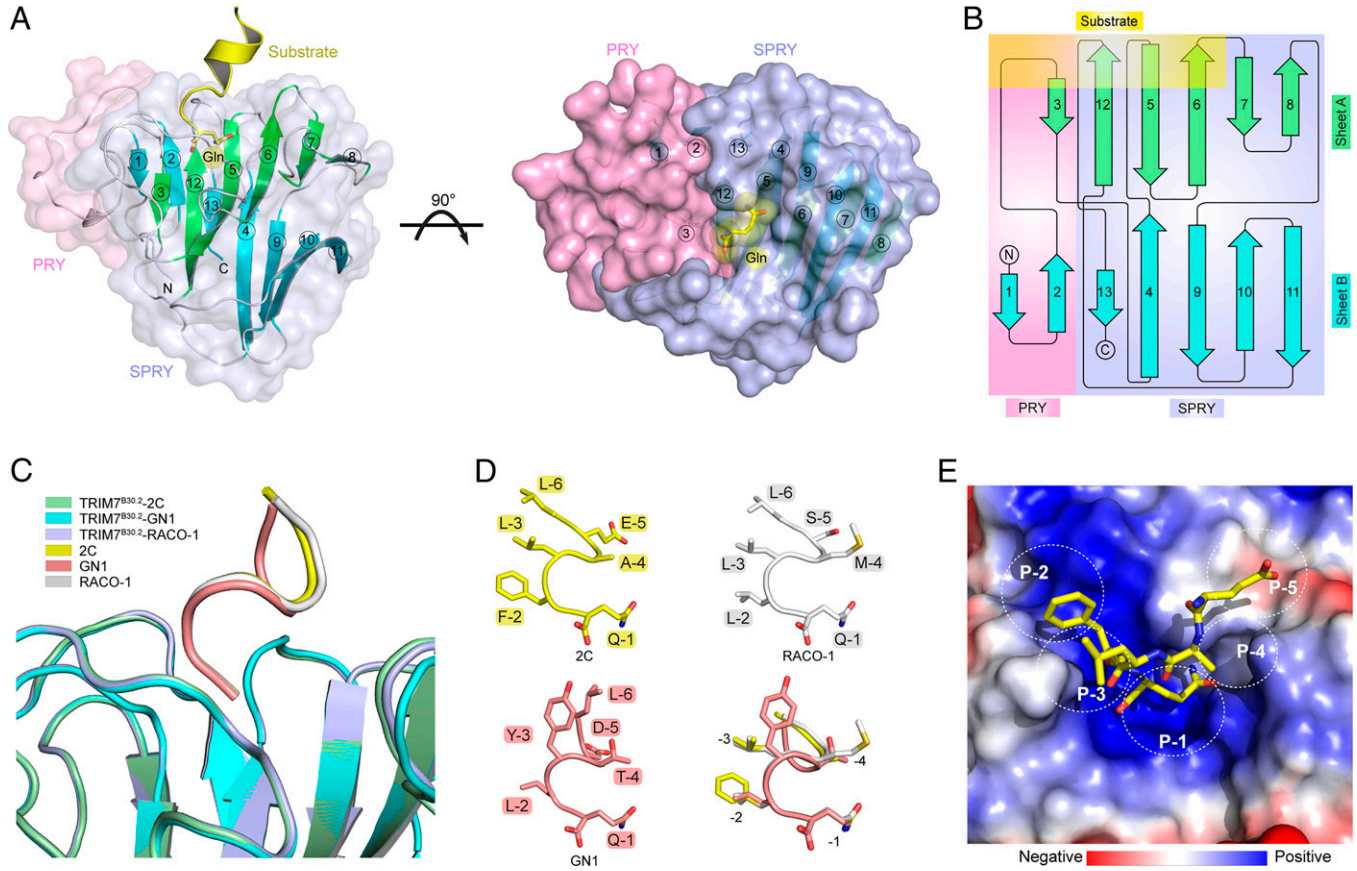

Fig. 2. Overall structures of TRIM7$^{B30.2}$ bound to the Gln/C-degron. (*A*) The structure of TRIM7$^{B30.2}$ bound to the 2C peptide in ribbon and surface views. In the ribbon view, sheet A and sheet B are colored green and cyan, respectively; in the surface view, PRY and SPRY subdomains are colored pink and light blue, respectively, and the substrate is colored yellow. (*B*) Topology diagram of the TRIM7 PRY-SPRY domain with the secondary elements colored as in *A*. (*C*) Superimposition of TRIM7$^{B30.2}$ bound to different peptides. (*D*) The Ct-residues of different substrates form a U-shaped conformation. (*E*) The electrostatic potential surface of the 2C-binding pocket in TRIM7$^{B30.2}$ (red, negative; blue, positive).

In addition, mutants of N383A, R385A, Q436A, and S499A, which would abolish the direct hydrogen bonds with Q−1, nearly abrogated the binding of the Gln/C-degron. We extended these observations by detecting interactions through a Co-IP assay, which showed that in contrast to wild-type (WT) TRIM7, the mutants of R385A, Q436A, and S499A completely precluded interactions with Q−1, consistent with our structure and ITC analyses (Fig. 4*E*).

To further dissect how TRIM7 directs the degradation of the Gln/C-degron, a cell-based ubiquitination assay was performed. Ectopically expressed Flag-tagged 2BC and mutant (Q−1A) were immunoprecipitated from HEK293T cells, and the ubiquitination levels of WT and mutant (Q−1A) were detected. The ubiquitination levels of WT 2BC dramatically increased upon TRIM7 overexpression, and 2BC protein levels subsequently decreased (Fig. 5*A*). In contrast, the ubiquitination levels and total protein levels of mutant (Q−1A) 2BC were not affected by TRIM7 overexpression (Fig. 5*B*). To further corroborate the importance of key residues of TRIM7 in mediating Gln/C-degron recognition, we detected the stabilization of Flag-tagged 2BC by constructing stable cell lines. The results showed that mutants of TRIM7 significantly attenuated the degradation of the 2BC protein compared to that of WT TRIM7 (Fig. 5*C* and *D*). In parallel, when we mutated Ct-Gln into Ala, the stability of 2BC was retained at a consistently high level with either overexpression of WT or mutants of TRIM7 (Fig. 5*E* and *F*). Taken together, these results established that the key residues of TRIM7-mediated Q−1 binding play a vital role in recognition and degradation of the 2BC protein through the Gln/C-degron pathway.

Structure Comparisons. Structural superposition of TRIM7$^{B30.2}$ in apo and peptide-bound states revealed that the overall structure of TRIM7$^{B30.2}$ did not undergo any major conformational rearrangements with an rmsd of 0.4 Å for the Cα atoms (*SI Appendix*, Fig. S5). Intriguingly, in the apo form, the potential Q−1 binding pocket of TRIM7$^{B30.2}$ was occupied by other ligands derived from crystallization conditions (41), in which one carboxyl group of malonate (MLI) was overlapped with the carboxyl group of Gln (*SI Appendix*, Fig. S5). The carboxyl groups of MLI and Gln were both stabilized by dual hydrogen bonds with the guanidine of Arg385 (*SI Appendix*, Fig. S5). In addition, the hydroxyl group of S,S-(2-hydroxyethyl)thiocysteine (CME501, Cys501 modified by β-mercaptoethanol) also pointed into the binding pocket of TRIM7$^{B30.2}$ (41), occupying the location of the side-chain carboxamide of Gln to further stabilize the globular structure (*SI Appendix*, Fig. S5).

By structural comparisons of TRIM7$^{B30.2}$-2C and TRIM21$^{B30.2}$-Fc complex modes, we found that the PRY and SPRY domains of TRIM21 possess their own discrete binding pockets for recognition of diverging domains of Fc homodimer, C_H2 and C_H3, in contrast to the single pocket of TRIM7$^{B30.2}$ constituted by the PRY and SPRY subdomains (*SI Appendix*, Fig. S6*A*). Distinct from the positively charged binding pocket of TRIM7$^{B30.2}$, the surface electronic charge of the two binding pockets in TRIM21$^{B30.2}$ was either electrically acidic or neutral

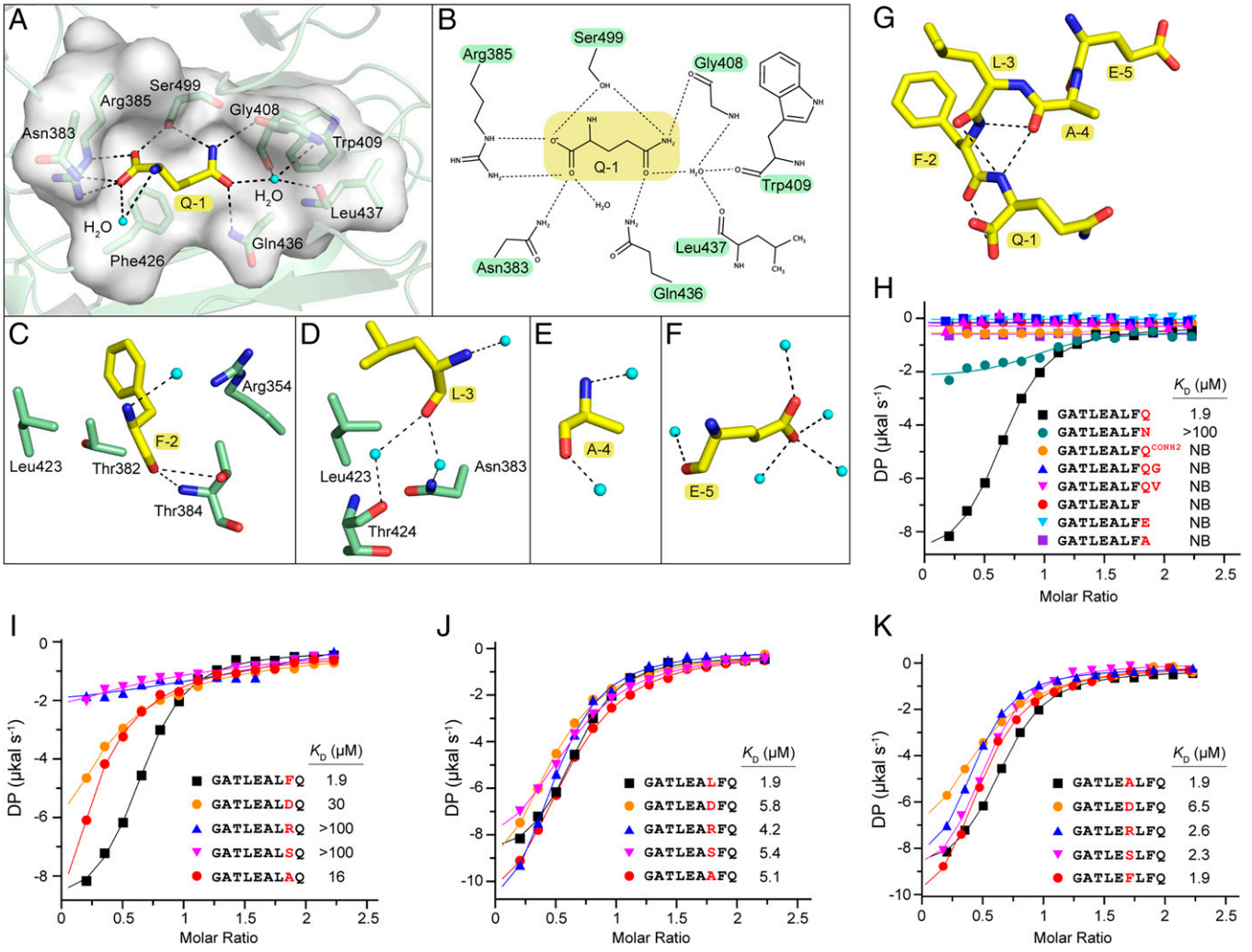

Fig. 3. Substrate selectivity and recognition of the Gln/C-degron by TRIM7$^{B30.2}$. (*A*) Closeup view of the interactions of TRIM7$^{B30.2}$ with Q−1 in the binding pocket. Q−1 is shown as yellow sticks; residues of TRIM7$^{B30.2}$ that are involved in the interactions are shown as pale green sticks. Water molecules are shown as cyan spheres. Hydrogen bonds are shown as black dashed lines. (*B*) A schematic illustration of the recognition of Q−1 by TRIM7$^{B30.2}$. (*C*–*F*) Closeup views of the interactions of F−2, L−3, A−4, and E-5 of the 2C peptide with TRIM7$^{B30.2}$. (*G*) The intramolecular interactions of the 2C peptide. (*H*–*K*) ITC fitting curves of TRIM7$^{B30.2}$ titrated by different peptides with position substitutions. The corresponding peptide sequences and binding affinities are indicated. DP, differential power; NB, no binding.

(*SI Appendix*, Fig. S6*B*). Additionally, hydrophobic stacking interactions played a more important role for substrate binding in TRIM21$^{B30.2}$ (42) instead of hydrogen bonding in TRIM7$^{B30.2}$.

Recently, the recognition mechanisms of KLHDC2-mediated Gly/C-degron and FEM1C-mediated Arg/C-degron have been described by structural studies (34, 43, 44). By comparing these binding modes, we found that these C-recognins all adopted positively charged binding pockets to accommodate limited-length substrates (*SI Appendix*, Fig. S7*A*). However, unlike KLHDC2 and FEM1C, whose C-degron–binding pockets are highly conserved, the binding pocket of TRIM7 exhibited a relative variable property (*SI Appendix*, Fig. S7*B*), hinting at the functional variety and specificity of various PRY-SPRY domain proteins in the physiological guarding of intracellular balance.

Discussion

As the major intracellular proteolytic system, the UPS regulates levels of oxidized, damaged, or misfolded proteins in eukaryotic cells (45, 46). E3 Ub ligases determine digestion specificity by recognizing the degrons of waste proteins (11, 12). To date, a series of *N*- and C-degron pathways has been reported (15, 18). In this study, we discovered a distinct C-degron pathway, the Gln/C-degron pathway, which can be specifically recognized by E3 ligase TRIM7$^{B30.2}$. We solved the crystal structures of TRIM7$^{B30.2}$ bound to different peptides bearing Ct-Gln and showed that TRIM7 utilizes the PRY and SPRY domains, forming a positively charged binding pocket to engage the U-shaped Gln/C-degron. The four Ct-residues of substrates are required for specific recognition by TRIM7$^{B30.2}$.

Recent studies have indicated that TRIM7 serves as an important antiviral effector that degrades the viral 2BC protein, impairing RNA replication of enteroviruses (37). However, a T323A mutation in CVB3 2C led to an obvious reduction in binding efficiency with TRIM7, with an increase in virus proliferation. Based on our structure, the T323 residue (its counterpart in the 2C degron peptide is T−7) is outside of the binding pocket of TRIM7$^{B30.2}$, making a minor contribution to direct binding. The T323A-mediated TRIM7 resistance is probably in part due to the fact that 2C ATPase activity depends on C terminus–mediated self-oligomerization, which is formed by interaction between the C terminus of one monomer and a hydrophobic pocket of the neighboring monomer. The mutation of T323 with hydrophobic

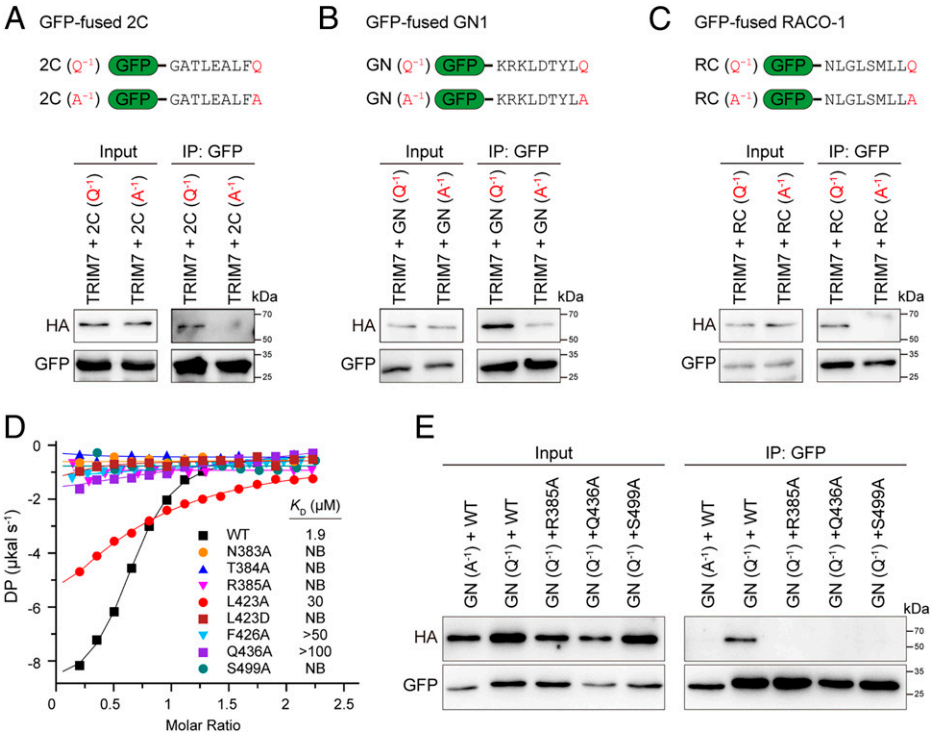

Fig. 4. Mutation analysis of substrate recognition by TRIM7. (*A*–*C*) Co-IP analysis of the interactions of TRIM7 with different Ct-peptides. HEK293T cells were cotransfected with HA-tagged TRIM7 (full-length) plasmid and GFP-fused WT and mutant 2C, GN1, or RACO-1 peptide plasmids. Cells were treated with MG132 (10 μM) for 6 h at 24 h after transfection and then harvested for Co-IP using anti-GFP beads and analyzed by Western blotting. (*D*) ITC fitting curves of WT and mutant TRIM7$^{B30.2}$ titrated with the 2C peptide. The corresponding mutations and binding affinities are indicated. (*E*) Co-IP analysis of the interactions of WT and indicated TRIM7 mutants with GFP-fused GN1 peptide. IP, immunoprecipitation; NB, no binding.

Ala would be more prone to dock into the hydrophobic pocket and promote the oligomerization of the 2C protein (37, 47), thereby protecting 2C from targeting by TRIM7. In our ITC assay (Fig. 1*D*), the T−7A nonapeptide, unlike the full-length 2C-T323A protein, was unable to form a self-oligomerization state. Therefore, the T-7A peptide has no discernable effect on TRIM7$^{B30.2}$ binding.

TRIM7 was shown to interact with RACO-1 and mediate its Lys63-linked ubiquitination in response to growth factor signaling (40). This modification thereby enhanced RACO-1 stability since RACO-1 is generally subject to autoubiquitination with Lys48-linked Ub and degradation by the proteasome (48). Herein, we suggest that the Ct-Gln of RACO-1 is responsible for its recognition by TRIM7$^{B30.2}$ and that this recognition might account for the Lys63-linked ubiquitination of RACO-1, while the detailed relationship still warrants further study.

Although few physiological substrates of TRIM7 have been reported so far, the UniProt database suggests that there are over 200 human proteins ending with the Gln/C-degron motif, indicating that TRIM7 may participate in a plethora of physiological processes. Additionally, somatic mutation scanning of TRIM7 in cancer samples revealed that a large number of mutations occur at the PRY-SPRY domain (*SI Appendix*, Fig. S8*A*). Among these, several mutants, including N383S, T384S, R385C, and L423P, are located at the key binding pocket of the Gln/C-degron (*SI Appendix*, Fig. S8*B*). Our ITC data also showed that these mutants strongly decreased TRIM7$^{B30.2}$–binding affinities against the 2C peptide (*SI Appendix*, Fig. S8*C*). In sum, our determination of the three-dimensional structure of TRIM7$^{B30.2}$ bound to specific ligands advances our understanding of TRIM7 and will facilitate, in particular, studies of its functions, including its role in mammalian responses to viral infections.

Materials and Methods

Bacteria. Two *Escherichia coli* (*E. coli*) strains were used in this study. *E. coli* strain T1 was used for DNA amplification and plasmid construction, and *E. coli* strain BL21 (DE3) was used for protein expression. Both were grown in Luria-Bertani medium (10 g tryptone, 5 g yeast extract, and 10 g NaCl per liter medium) at 37 °C.

Human Cells. HEK293T cells (American Type Culture Collection [ATCC], CRL-3216) were cultured in Dulbecco's Modified Eagle's Medium (DMEM; Cellgro) with the addition of 1% penicillin/streptomycin and 10% fetal bovine serum (FBS; BioInd) inside a 37 °C incubator with humidified atmosphere of 5% CO_2.

Protein Expression and Purification. The PRY-SPRY domains of human TRIM7$_{338-511}$, TRIM7$_{338-511}$-linker (GGSGGSSV)-2C (GATLEALFQ), TRIM7$_{338-511}$-linker (GGSGGSGG)-GN1 (GAKLDTYLQ), TRIM7$_{338-511}$-linker (GGSGGSGGSSV)-RACO-1 (GATLSMLLQ), and 2C$_{116-329}$ were cloned into pET28-MKH8SUMO vector (Addgene Plasmid #79526). The recombinant plasmid was transformed into *E. coli* BL21 (DE3) for induced expression with 0.2 mM isopropyl β-D-1-thiogalactopyranoside at 18 °C overnight. The bacteria were harvested by centrifugation, and the pellets were resuspended in buffer containing 20 mM Tris·HCl, pH 8.5, 400 mM NaCl, and 2 mM β-mercaptoethanol. Cells were lysed by sonication on ice. Cell debris was removed by centrifugation at 14,000 rpm for 40 min at 4 °C. The supernatant was loaded into Ni-NTA (GE Healthcare), and untagged protein was washed by washing buffer (20 mM Tris·HCl, pH 8.5, 400 mM NaCl, and 25 mM imidazole, pH 8.5). The target protein was eluted by elution buffer (20 mM Tris·HCl, pH 8.5, 400 mM NaCl, and 500 mM imidazole, pH 8.5). The 8×His-SUMO tag was cleaved by TEV protease with a molar ratio of 1:20 in dialysis buffer (20 mM Tris·HCl, pH 8.5, 500 mM NaCl, and 2 mM β-mercaptoethanol) at 4 °C overnight. Then the protein sample was reloaded onto an Ni-NTA column to remove TEV protease and cleaved 8×His-SUMO tag. Protein was further purified by size exclusion chromatography (Superdex 200 Increase 10/300 GL, GE Healthcare). The purified protein was concentrated and stored at −80 °C for later use. The mutants were generated by standard PCR-based mutagenesis

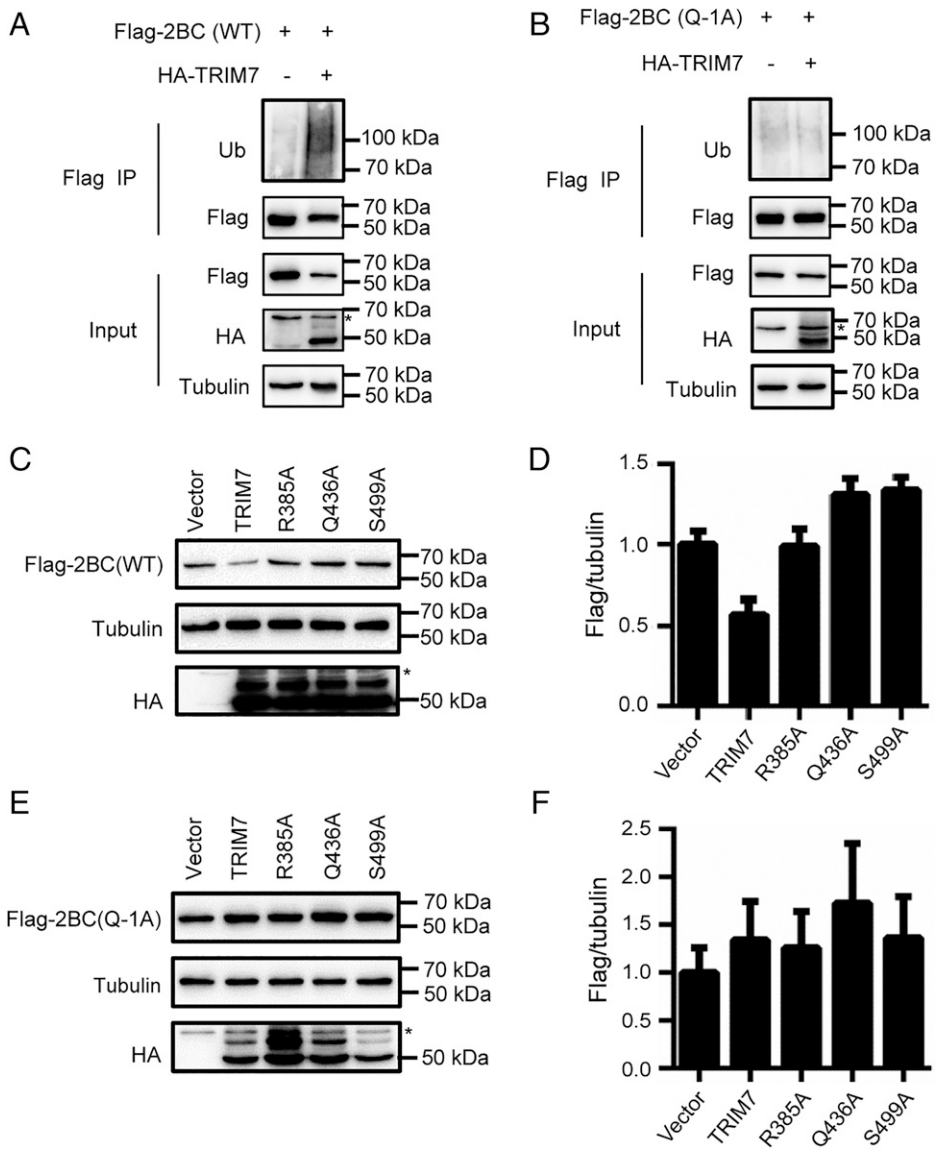

Fig. 5. TRIM7 mediates the degradation of 2BC protein. (*A* and *B*) Ubiquitination assay for WT Flag-tagged 2BC (full-length) and mutant. HEK293T cells were cotransfected for 48 h with HA-TRIM7 and Flag-2BC (full-length) or mutant (Q−1A) plasmids. Cells were harvested for IP using anti-Flag beads and analyzed by Western blot. (*C*) Western blotting analysis of Flag-2BC (WT) stability. HEK293T cells were coinfected with Flag-2BC-WT lentivirus and indicated WT and mutant HA-TRIM7 lentivirus. The infected cells were selected with blasticidin (10 μg mL^{-1}) and puromycin (2 μg mL^{-1}) for 3 to 4 d. Then cells were harvested and analyzed by Western blot. (*D*) Relative protein level quantified by ImageJ software corresponding to *C*. The results are the mean value averaged from three independent experiments. Error bars, SD. (*E*) Western blotting analysis of Flag-2BC (Q−1A) stability. (*F*) Relative protein level quantified by ImageJ software corresponding to *E*. The results are the mean value averaged from three independent experiments. Error bars, SD. Asterisk (*) indicates nonspecific binding of the antibodies to another nonspecific protein of this size. IP, immunoprecipitation.

using $TRIM7_{338-511}$ as a template and verified by DNA sequencing. Expression and purification of the mutant proteins were similar to that of the WT protein.

Protein Crystallization. Crystals were obtained using the sitting-drop vapor-diffusion method at 18 °C by equilibrating 1 μL protein solution (5 mg mL^{-1} in 20 mM Tris·HCl, pH 8.5, 150 mM NaCl, and 1 mM dithiothreitol [DTT]) mixed with 1 μL reservoir solution. Crystallization conditions were as follows:

1) $TRIM7_{338-511}$-2C: 0.1 M sodium formate, pH 7.0, 20% (wt/vol) polyethylene glycol 3,350, and 0.2 M NaCl;
2) $TRIM7_{338-511}$-GN1: 0.1 M 4-Morpholineethanesulfonic acid monohydrate, pH 6.0, and 14% (wt/vol) polyethylene glycol 4,000;
3) $TRIM7_{338-511}$-RACO-1: 0.2 M potassium sodium tartrate tetrahydrate and 26% (wt/vol) polyethylene glycol 3,350.

Data Collection and Structure Determination. Diffraction data were collected on beamline BL02U or BL17B at the Shanghai Synchrotron Radiation Facility and processed with the program package XDS (X-ray detector software) (49). All structures were solved by molecular replacement with Phaser by using the TRIM7 B30.2 domain (Protein Data Bank code 6UMA) as a template. The models were refined with PHENIX (50) and rebuilt with Coot (51). All structural figures were generated by Pymol (https://www.pymol.org/2/).

ITC Assay. ITC assays were carried out on a MicroCal PEAQ-ITC instrument (Malvern Panalytical) at 16 °C. All proteins and peptides were dissolved in the ITC buffer consisting of 20 mM Tris·HCl, pH 8.5, and 150 mM NaCl. Each ITC experiment was performed by titrating of 1.5 μL peptide (1 to 2 mM) or protein solution (0.9 mM) into 30 to 50 μM protein solution, with a spacing time of 90 s and a reference power of 10 μCal/s. The titration data were analyzed using the one-site binding model from MicroCal PEAQ-ITC Analysis Software version 1.30. All ITC assays were repeated at least twice independently with similar results.

GST Pull-down Assay. GST or GST-fused C-degrons were produced by *E. coli* BL21 (DE3) cells and purified using GST and Superdex 200 Increase–sized exclusion columns. Approximately 100 μg purified GST or GST-fused C-degron and 200 μg purified $TRIM7^{B30.2}$ were used to perform each GST pull-down

assay. About 200 μL reaction mixtures was incubated with 20 μL beads in the binding buffer (20 mM Tris·HCl, pH 7.5, 150 mM NaCl, and 1 mM DTT) at 4 °C for 1 h. After three extensive washings with 400 μL binding buffer, the pull-down samples were eluted with 50 mM glutathione and analyzed by sodium dodecyl sulfate polyacrylamide gel electrophoresis (SDS-PAGE) followed by Coomassie Blue staining.

Cell Culture and Viral Transduction. The human HEK293T (ATCC, CRL-3216) cell line was maintained in DMEM (Cellgro) supplemented with 10% FBS (BioInd) and 1% penicillin/streptomycin. For lentiviral production, HEK293T cells were cotransfected with pMD2.G (Addgene #12259), psPAX2 (Addgene #12260) or pCDH-CMV (Addgene #72265) constructs. After 48-h culturing, the viral particle supernatants were collected and applied for infection of HEK293T cells with the presence of 8 μg mL^{-1} polybrene. Forty-eight hours later, the infected cells were selected with the addition of blasticidin (10 μg mL^{-1}) and/or puromycin (2 μg mL^{-1}) for pCDH clones for 3 to 4 d before the following experiments.

Cell Lysate Extraction and Co-IP. The whole-cell lysate extracts were prepared from HEK293T cells. Two days after transient transfection, cells were collected and resuspended in cell lysis buffer (50 mM Tris·HCl, pH 7.4, 250 mM NaCl, 0.5% Triton X-100, 10% glycerol, 1 mM freshly added DTT, 1 mM PMSF (phenylmethanesulfonyl fluoride), and protease inhibitors). Approximately 1 mg of the whole-cell lysate was incubated with GFP (green fluorescent protein)-Trap Magnetic Particles (Proteintech) or anti-Flag M2 magnetic beads (Sigma-Aldrich) overnight at 4 °C. Then the beads were washed four times with the same cell lysis buffer and resolved proteins from beads with 100 μL of 2×SDS sample buffer. The sample was boiled for 5 to 10 min and then analyzed using SDS-PAGE and Western blotting. The following antibodies were used for immunoblotting: anti-HA (1:1,000; Proteintech, 51064–2-AP), anti-GFP (1:5,000; Proteintech, 50430–2-AP), anti-Flag (1:1,000; Proteintech, 20543–1-AP), anti-Ub (1:1,000; Cell Signaling, #3933), and anti-tubulin (1:5,000; Proteintech, 11224–1-AP).

Cell-Based Ubiquitination Assay. HEK293T cells were cotransfected for 48 h with HA-TRIM7 and Flag-2BC (full-length) or mutant (Q—1A) plasmids. Cells were collected and resuspended in RIPA Buffer (50 mM Tris·HCl, pH 7.4, 150 mM NaCl, 2 mM EDTA (ethylene diamine tetraacetic acid), 1% Nonidet P-40, 0.1% SDS, 1 mM PMSF, and protease inhibitors). Approximately 1 mg of the whole-cell lysate was incubated with anti-Flag M2 magnetic beads (Sigma-Aldrich) overnight at 4 °C. Then the beads were washed four times with the same lysis buffer and resolved proteins from beads with 100 μL of 2×SDS sample buffer. Then ubiquitination was analyzed using SDS-PAGE and Westernblotting.

Data Availability. The atomic coordinates and structure factors of $TRIM7^{B30.2}$-2C, $TRIM7^{B30.2}$-GN1, and $TRIM7^{B30.2}$RACO-1 complexes have been deposited in the Protein Data Bank (https://www.rcsb.org/) under the accession codes 7Y3A (52), 7Y3B (53), and 7Y3C (54). All study data are included in the article and/or *SI Appendix*.

ACKNOWLEDGMENTS. We thank the staff at beamlines BL02U and BL17B of the Shanghai Synchrotron Radiation Facility for assistance with X-ray data collection. This work was supported by National Natural Science Foundation of China Grant Nos. 31900865 (to C.D.), 32071193 (to C.D.), 81974431 (to W.M.), 82173000 (to W.M.), and 81874039 (to X.Y.), and by the Haihe Laboratory of the Cell Ecosystem Innovation Fund.

Author affiliations: [a]Haihe Laboratory of Cell Ecosystem, The Province and Ministry Co-sponsored Collaborative Innovation Center for Medical Epigenetics, Key Laboratory of Immune Microenvironment and Disease (Ministry of Education), Tianjin Medical University General Hospital, The Second Hospital of Tianjin Medical University, Tianjin Medical University, Tianjin, 300070, China; [b]Department of Genetics, School of Basic Medical Sciences, Tianjin Medical University, Tianjin, 300070, China; [c]Department of Biochemistry and Molecular Biology, School of Basic Medical Sciences, Tianjin Medical University, Tianjin, 300070, China; and [d]The Province and Ministry Co-sponsored Collaborative Innovation Center for Medical Epigenetics, Key Laboratory of Immune Microenvironment and Disease (Ministry of Education), Tianjin Key Laboratory of Cellular and Molecular Immunology, Department of Immunology, Tianjin Medical University, Tianjin, 300070, China

1. D. Balchin, M. Hayer-Hartl, F. U. Hartl, In vivo aspects of protein folding and quality control. *Science* **353**, aac4354 (2016).
2. T. Ravid, M. Hochstrasser, Diversity of degradation signals in the ubiquitin-proteasome system. *Nat. Rev. Mol. Cell Biol.* **9**, 679–690 (2008).
3. S. Shao, R. S. Hegde, Target selection during protein quality control. *Trends Biochem. Sci.* **41**, 124–137 (2016).
4. E. M. Sontag, R. S. Samant, J. Frydman, Mechanisms and functions of spatial protein quality control. *Annu. Rev. Biochem.* **86**, 97–122 (2017).
5. I. Tripathi-Giesgen, C. Behrends, A. F. Alpi, The ubiquitin ligation machinery in the defense against bacterial pathogens. *EMBO Rep.* **22**, e52864 (2021).
6. D. Popovic, D. Vucic, I. Dikic, Ubiquitination in disease pathogenesis and treatment. *Nat. Med.* **20**, 1242–1253 (2014).
7. D. Senft, J. Qi, Z. A. Ronai, Ubiquitin ligases in oncogenic transformation and cancer therapy. *Nat. Rev. Cancer* **18**, 69–88 (2018).
8. Y. Watanabe, K. Taguchi, M. Tanaka, Ubiquitin, autophagy and neurodegenerative diseases. *Cells* **9**, 2022 (2020).
9. D. Finley, Recognition and processing of ubiquitin-protein conjugates by the proteasome. *Annu. Rev. Biochem.* **78**, 477–513 (2009).
10. Y. T. Kwon, A. Ciechanover, The ubiquitin code in the ubiquitin-proteasome system and autophagy. *Trends Biochem. Sci.* **42**, 873–886 (2017).
11. C. E. Berndsen, C. Wolberger, New insights into ubiquitin E3 ligase mechanism. *Nat. Struct. Mol. Biol.* **21**, 301–307 (2014).
12. L. Buetow, D. T. Huang, Structural insights into the catalysis and regulation of E3 ubiquitin ligases. *Nat. Rev. Mol. Cell Biol.* **17**, 626–642 (2016).
13. N. Zheng, N. Shabek, Ubiquitin ligases: Structure, function, and regulation. *Annu. Rev. Biochem.* **86**, 129–157 (2017).
14. A. Bachmair, D. Finley, A. Varshavsky, In vivo half-life of a protein is a function of its amino-terminal residue. *Science* **234**, 179–186 (1986).
15. A. Varshavsky, N-degron and C-degron pathways of protein degradation. *Proc. Natl. Acad. Sci. U.S.A.* **116**, 358–366 (2019).
16. H. C. Lin *et al.*, C-terminal end-directed protein elimination by CRL2 ubiquitin ligases. *Mol. Cell* **70**, 602–613.e3 (2018).
17. I. Koren *et al.*, The eukaryotic proteome is shaped by E3 ubiquitin ligases targeting C-terminal degrons. *Cell* **173**, 1622–1635.e14 (2018).
18. R. T. Timms, I. Koren, Tying up loose ends: The N-degron and C-degron pathways of protein degradation. *Biochem. Soc. Trans.* **48**, 1557–1567 (2020).
19. A. Varshavsky, The N-end rule pathway and regulation by proteolysis. *Protein Sci.* **20**, 1298–1345 (2011).
20. A. Yesbolatova, M. T. Kanemaki, Understanding the Pro/N-end rule pathway. *Nat. Chem. Biol.* **14**, 414–415 (2018).
21. C. S. Hwang, A. Shemorry, D. Auerbach, A. Varshavsky, The N-end rule pathway is mediated by a complex of the RING-type Ubr1 and HECT-type Ufd4 ubiquitin ligases. *Nat. Cell Biol.* **12**, 1177–1185 (2010).
22. M. Pan *et al.*, Structural insights into Ubr1-mediated N-degron polyubiquitination. *Nature* **600**, 334–338 (2021).
23. J. Chrustowicz *et al.*, Multifaceted N-degron recognition and ubiquitylation by GID/CTLH E3 ligases. *J. Mol. Biol.* **434**, 167347 (2022).
24. C. Dong *et al.*, Molecular basis of GID4-mediated recognition of degrons for the Pro/N-end rule pathway. *Nat. Chem. Biol.* **14**, 466–473 (2018).
25. A. Melnykov, S. J. Chen, A. Varshavsky, Gid10 as an alternative N-recognin of the Pro/N-degron pathway. *Proc. Natl. Acad. Sci. U.S.A.* **116**, 15914–15923 (2019).
26. J. S. Shin, S. H. Park, L. Kim, J. Heo, H. K. Song, Crystal structure of yeast Gid10 in complex with Pro/N-degron. *Biochem. Biophys. Res. Commun.* **582**, 86–92 (2021).
27. X. Yan *et al.*, Molecular basis for recognition of Gly/N-degrons by $CRL2^{ZYG11B}$ and $CRL2^{ZER1}$. *Mol. Cell* **81**, 3262–3274.e3 (2021).
28. Y. Liu, C. Liu, W. Dong, W. Li, Physiological functions and clinical implications of the N-end rule pathway. *Front. Med.* **10**, 258–270 (2016).
29. S. M. Sriram, B. Y. Kim, Y. T. Kwon, The N-end rule pathway: Emerging functions and molecular principles of substrate recognition. *Nat. Rev. Mol. Cell Biol.* **12**, 735–747 (2011).
30. H. Hu, S. C. Sun, Ubiquitin signaling in immune responses. *Cell Res.* **26**, 457–483 (2016).
31. H. Ashida, C. Sasakawa, Bacterial E3 ligase effectors exploit host ubiquitin systems. *Curr. Opin. Microbiol.* **35**, 16–22 (2017).
32. K. S. Robinson *et al.*, Enteroviral 3C protease activates the human NLRP1 inflammasome in airway epithelia. *Science* **370**, eaay2002 (2020).
33. A. Chatr-Aryamontri, A. van der Sloot, M. Tyers, At long last, a C-terminal bookend for the ubiquitin code. *Mol. Cell* **70**, 568–571 (2018).
34. X. Yan *et al.*, Molecular basis for ubiquitin ligase $CRL2^{FEM1C}$-mediated recognition of C-degron. *Nat. Chem. Biol.* **17**, 263–271 (2021).
35. S. Hatakeyama, TRIM family proteins: Roles in autophagy, immunity, and carcinogenesis. *Trends Biochem. Sci.* **42**, 297–311 (2017).
36. K. Ozato, D. M. Shin, T. H. Chang, H. C. Morse III, TRIM family proteins and their emerging roles in innate immunity. *Nat. Rev. Immunol.* **8**, 849–860 (2008).
37. W. Fan *et al.*, TRIM7 inhibits enterovirus replication and promotes emergence of a viral variant with increased pathogenicity. *Cell* **184**, 3410–3425.e17 (2021).
38. A. Hage, R. Rajsbaum, To TRIM or not to TRIM: The balance of host-virus interactions mediated by the ubiquitin system. *J. Gen. Virol.* **100**, 1641–1662 (2019).
39. A. V. Skurat, A. D. Dietrich, L. Zhai, P. J. Roach, GNIP, a novel protein that binds and activates glycogenin, the self-glucosylating initiator of glycogen biosynthesis. *J. Biol. Chem.* **277**, 19331–19338 (2002).
40. A. Chakraborty, M. E. Diefenbacher, A. Mylona, O. Kassel, A. Behrens, The E3 ubiquitin ligase Trim7 mediates c-Jun/AP-1 activation by Ras signalling. *Nat. Commun.* **6**, 6782 (2015).
41. C. J. Muñoz Sosa, F. M. Issoglio, M. E. Carrizo, Crystal structure and mutational analysis of the human TRIM7 B30.2 domain provide insights into the molecular basis of its binding to glycogenin-1. *J. Biol. Chem.* **296**, 100772 (2021).
42. L. C. James, A. H. Keeble, Z. Khan, D. A. Rhodes, J. Trowsdale, Structural basis for PRYSPRY-mediat motif (TRIM) protein function. *Proc. Natl. Acad. Sci. U.S.A.* **104**, 6200–6205 (2007).
43. X. Chen *et al.*, Molecular basis for arginine C-terminal degron recognition by $Cul2^{FEM1}$ E3 ligase. *Nat. Chem. Biol.* **17**, 254–262 (2021).
44. D. V. Rusnac *et al.*, Recognition of the diglycine C-end degron by $CRL2^{KLHDC2}$ ubiquitin ligase. *Mol. Cell* **72**, 813–822.e4 (2018).

45. I. Amm, T. Sommer, D. H. Wolf, Protein quality control and elimination of protein waste: The role of the ubiquitin-proteasome system. *Biochim. Biophys. Acta* **1843**, 182–196 (2014).
46. J. L. Sun-Wang, S. Ivanova, A. Zorzano, The dialogue between the ubiquitin-proteasome system and autophagy: Implications in ageing. *Ageing Res. Rev.* **64**, 101203 (2020).
47. H. Guan *et al.*, Crystal structure of 2C helicase from enterovirus 71. *Sci. Adv.* **3**, e1602573 (2017).
48. C. C. Davies *et al.*, Identification of a co-activator that links growth factor signalling to c-Jun/AP-1 activation. *Nat. Cell Biol.* **12**, 963–972 (2010).
49. W. Kabsch, XDS. *Acta Crystallogr. D Biol. Crystallogr.* **66**, 125–132 (2010).
50. D. Liebschner *et al.*, Macromolecular structure determination using X-rays, neutrons and electrons: Recent developments in Phenix. *Acta Crystallogr. D Struct. Biol.* **75**, 861–877 (2019).
51. P. Emsley, B. Lohkamp, W. G. Scott, K. Cowtan, Features and development of Coot. *Acta Crystallogr. D Biol. Crystallogr.* **66**, 486–501 (2010).
52. Y. Ru *et al.*, Atomic coordinates and structure factors for "C-terminal glutamine acts as a C-degron targeted by E3 ubiquitin ligase TRIM7." Accession # 7Y3A. Protein Data Bank. https://www.rcsb.org/structure/unreleased/7Y3A. Deposited 10 June 2022.
53. Y. Ru *et al.*, Atomic coordinates and structure factors for "C-terminal glutamine acts as a C-degron targeted by E3 ubiquitin ligase TRIM7." Accession # 7Y3B. Protein Data Bank. https://www.rcsb.org/structure/unreleased/7Y3B. Deposited 10 June 2022.
54. Y. Ru *et al.*, Atomic coordinates and structure factors for "C-terminal glutamine acts as a C-degron targeted by E3 ubiquitin ligase TRIM7." Accession # 7Y3C. Protein Data Bank. https://www.rcsb.org/structure/unreleased/7Y3C. Deposited 10 June 2022.